Article

A Numerical Study on Fuel Injection Optimization for a ME-GI Dual-Fuel Marine Engine Based on CFD Analysis

Jun-Soo Kim [1] , Won-Ju Lee [2,3] , Van Chien Pham [3,*] and Jae-Hyuk Choi [2,*]

1 Korea Institute of Maritime and Fisheries Technology, 367, Haeyang-ro, Yeongdo-gu, Busan 49111, Korea; jskim@seaman.or.kr

2 Division of Marine System Engineering, Korea Maritime and Ocean University, 727, Taejong-ro, Yeongdo-gu, Busan 49112, Korea; skywonju@kmou.ac.kr

3 Interdisciplinary Major of Maritime AI Convergence, Korea Maritime and Ocean University, 727, Taejong-ro, Yeongdo-gu, Busan 49112, Korea

* Correspondence: chien.pham@ut.edu.vn (V.C.P.); choi_jh@kmou.ac.kr (J.-H.C.); Tel.: +82-10-4254-1142 (V.C.P.); +82-51-410-4257 (J.-H.C.)

Abstract: A numerical study was carried out to investigate the effects of injector spray angle (SA) and injection position (IP) on the combustion and emission characteristics of a two-stroke ME-GI marine engine at full load. Three-dimensional (3D) simulations of the combustion process and emission formations inside the cylinder of the engine operating in the diesel and DF modes were performed using the ANSYS Fluent simulation software to analyze the in-cylinder pressure, temperature, and emission characteristics. The simulation results were compared and showed good agreement with the experimental results reported in the engine's shop test technical data. The simulation results showed that the IP of 0.02 m with an SA of 40 degrees helps to enhance the engine performance; however, if the main target is reducing engine exhaust gas emissions, an IP of 0.01 m is highly recommended to be used. At this IP, the specific SA of 40, 45, or 50 degrees that should be used will depend on which emissions (NO, soot, CO_2, etc.) need to be reduced. This study successfully investigated the effects of injector SA and IP on the combustion and emission characteristics of the researched engine and would be a good reference for engine design and operating engineers.

Keywords: injector spray angle; ME-GI engine; dual-fuel (DF) engine; combustion; exhaust gas emission; simulation; computational fluid dynamic (CFD) analysis

1. Introduction

To limit the impact of emissions on human health and the Earth's environment, the marine emission regulations released by the International Maritime Organization (IMO) are becoming increasingly strict. In order to meet these stricter emission regulations, emission reduction solutions are mandatorily applied on both new-build and existing ships nowadays [1–3]. According to the MARPOL (International Convention for the Prevention of Pollution from Ships) Annex VI, since 1 January 2020, all ships have to comply with the utilization of fuels with max. 0.5% sulfur globally. The minimum reduction in carbon intensity per maritime transport work must reach 40% by 2030 compared with 2008, with the target of reaching 70% by 2050. The reduction in greenhouse gas (GHG) emissions from marine shipping must reach at least 50% by 2050 compared with 2008. From 2016, NOx emissions from ships have been limited to 3.4 g/kWh for engines with speeds less than or equal to 130 rpm. This limit gradually decreases with increasing engine speed and reaches only 2 g/kWh for engines with a speed higher than or equal to 2000 rpm [4]. There are various solutions for reducing emissions from marine engines, but this paper focuses on two aspects: engine technologies and alternative fuels.

Among combustion engines, internal combustion engines (ICEs) with their high thermal efficiency have been widely used in industry. Among ICEs, compression ignition (CI)

diesel engines have higher thermal efficiency compared to spark ignition (SI) gasoline engines [5]. They are therefore currently contributing a very large portion in providing propulsion for propellers as well as generators on ships. However, EGEs such as NOx (nitrogen oxides), soot, and CO_2 (carbon dioxide—one of the strong greenhouse gases—GHGs) produced from the combustion process of such engines are major concerns nowadays.

In ICEs, the combustion of fuel by the O_2 (oxygen) present in the supplied air inside the engine combustion chamber generates engine power, while also producing EGEs. Therefore, engine performance and EGE characteristics are greatly influenced by the fuel type, fuel-supplying method, fuel injection characteristics, fuel–air equivalent ratio, fuel–air mixing quality, combustion chamber geometry, etc. [6]. Among many kinds of fuels, natural gas (NG), which principally consists of methane (CH_4), has been and will still be widely used in heavy-duty marine engines. It has many advantages, such as low EGEs, low price, no processing, abundant reserves, etc. However, since NG has a high self-ignition temperature (low cetane numbers), it needs an external energy source for ignition, such as a spark plug in SI engines or pilot diesel oil in dual-fuel (DF) engines. If NG is used in the DF engines, pure diesel engines can be modified to an NG–diesel DF engine very easily and with only a low cost [7–9]. Numerous studies have been performed to investigate the combustion and EGE characteristics of NG–diesel DF engines [10]. The detailed properties, as well as the effects of NG on the combustion and EGE characteristics of an NG–diesel DF engine, can also be referred to in our previous studies [11,12].

Regarding engine technologies, ME-GI (M-type, Electronically Controlled Gas Injection) engines designed by MAN B&W are one of the state-of-the-art engines in the maritime industry today. In total, more than 200 engines have been ordered and in use since 2015, and the number will rapidly increase in the coming years [13]. Unlike the DF engines, which use intake port injection for primary gas introduction, ME-GI DF engines use the direct injection method for the primary gas introduction. The gaseous fuel is injected and burned directly, leading to high efficiency and combustion stability according to the diesel cycle principle. With direct gas injection, the injection timing, gas injection rate, and injection pressure can be controlled in a wide range of engine loads and speeds to keep the optimal spraying quality. This is considered to be one of the most important and necessary factors to achieve better combustion efficiency [14]. Furthermore, the engines designed according to the diesel cycle principle allow the operators to switch smoothly between different fuel modes, i.e., the fuel oil and DF mode [13].

Through the above analysis, the combination of using cleaner NG fuel and fuel direct injection technology in ME-GI DF engines provides an extremely effective solution for reducing EGEs from ships. To maximize the advantages of ME-GI engines, operators need to have insight into the influence of operating parameters on the engine. However, because the ME-GI engine family is so new, not much research has been done on these engines. In addition, the parameters related to the structure and layout of the fuel injectors in the combustion chamber are confidential documents of companies, so they should always be carefully preserved to avoid technology theft. As a result, it is impossible for engine operators to access these documents. This study aims to analyze the effectiveness of using NG as the primary fuel in ME-GI DF engines and the impacts of some of the main parameters of the fuel injector on the combustion and emission formation of the engine. This research will help engine designers and operators to be aware of the key factors that greatly impact engine power and emissions so that they can design and operate engines more efficiently.

In fuel direct-injection engines, the diffusion combustion phase accounts for most of the engine's combustion process. In this phase of combustion, the mixing quality between the injected fuel and supplied air inside the engine combustion chamber strongly affects the rate of heat release (RoHR) and the formation of harmful emissions. Ideally, all the injected fuel will be in contact with all the oxygen available in the combustion chamber so that the combustion of fuel can take place as completely as possible. Both the fuel injection characteristics and atomization are the major factors in improving engine power

while reducing EGEs [6]. Regarding the fuel injection characteristics, the injection method (port- or direct-injection), injection timing, injection strategy (single- or multiple-injection), SA, and IP play important roles in the combustion and EGE characteristics of engines. In fuel direct-injection engines, SA and IP have great influences on the combustion and EGE formation of the engine as they determine the fuel injection targeting point in the combustion chamber [5]. Therefore, studies for SA and IP are very important and will have implications for both engine design and operating engineers.

Regarding the multiple-injection strategy, a series of studies have been carried out and demonstrated the effectiveness of this strategy in reducing soot or even soot and NOx (nitrogen oxides) emissions simultaneously in heavy-duty direct-injection diesel engines [15–19]. A systematic analysis of the mechanisms of droplet breakup and mixing with the surrounding fluid of fluid injection, and its relation to vorticity generation and transport, has been reported and can be referred to [20]. The effectiveness of the double-injection strategy in reducing EGEs applied on a heavy-duty direct-injection diesel marine engine has also been demonstrated and can be referenced in our previous study [21].

Maghbouli et al. reported in [22] that the nozzle axial location, which determines IP, considerably affected both the in-cylinder pressure and EGEs of fuel direct-injection engines. Here, a change in the axial location of the fuel nozzle by only a few millimeters led to a considerable change in the engine performance and emission behavior. Mobasheri and Peng reported in [23] that the narrow-spray-angle injection helped to reduce the NOx and soot emissions without affecting the fuel oil consumption due to improved fuel–air mixture quality. Yoon et al. studied the effect of SA and fuel injection strategy on the combustion and emission characteristics of a direct-injection engine operating with dimethyl ether (DME). Through the study, they found that the in-cylinder peak pressure in the single-injection strategy using narrow-spray-angle injection (60 and 70 degrees) with advanced fuel injection timing was increased compared to that in the wide-spray-angle injection (156 degrees) with later injection timing [24]. In direct-injection CI diesel engines, the target injection point in the engine's combustion chamber is very important because it causes wetting of the combustion chamber walls, which causes the formation of unburnt hydrocarbons (UHC). Additionally, the consumption of O_2 in the combustion process also greatly depends on the targeting point [25–27]. Furthermore, rapid combustion in fuel-rich regions inside engine combustion chambers causes the deterioration of the combustion efficiency, knocking phenomenon, and high levels of NOx emissions from the engine. Therefore, many researchers have tried to determine the optimal SA [28–31]. Fang et al. reported in [31] that using narrow-angle injection with a 70-degree SA led to higher soot formation due to the deposition of the fuel film on the piston wall. It, however, lowers NOx emissions because of the leaner fuel–air mixture near the piston surface. Shu et al. used the computational fluid dynamic (CFD) method coupled with a chemical kinetic model to investigate the emission characteristics of an NG–diesel DF engine at various SA [7]. They concluded that NOx emissions increased by 93% when the fuel injector SA increased from 60 to 140 degrees but decreased by 15% when the SA was further increased to 160 degrees. Lim and Min performed a CFD analysis in a diesel engine operating with various SAs in order to reduce soot and minimize wall impingement [32]. They found that at the SA of 100 degrees, soot was reduced by 41% compared to that in the case of the SA of 70 degrees.

From the above literature review, it is very important to note that although many studies have been carried out on NG–diesel DF engines to investigate the effect of SA on the combustion and emission characteristics of the engine, studies on the effect of SA and IP on NG–diesel ME-GI DF marine engines are very rare. The authors have reviewed a wide variety of literature but still have not found any studies similar to the one in this report.

In this study, the effect of SA and IP on the combustion process and emission characteristics of an NG–diesel ME-GI DF marine engine was investigated by using the CFD method coupled with a reduced chemical kinetic model. The combustion and emission formation occurring inside the engine cylinder were modeled by using the ANSYS Fluent code. The ultimate target of this study was to specify the optimal SA and IP for the engine.

The CFD models were validated by the experimental results reported in the engine's shop test technical data. The study also successfully assigned the optimal SA and IP for the engine to achieve certain emission reductions.

2. Numerical Analysis

The ANSYS Fluent 2019R2 software, with its advanced models, was used to simulate the combustion and emission formations that occur inside the engine cylinder. The working process of the engine was modeled from the Scavenge Port Closing (SPC) to the Exhaust Valve Opening (EVO). The simulation process included three steps: (1) pre-processing, (2) processing, and (3) post-processing. The first step included building the computational domain (Geometry), creating movable computational meshes (Meshing), and setting up the simulation parameters (Setup). The solutions were calculated in the second step. In the third step, the simulation results were analyzed and reported. After obtaining the simulation results, the simulation and experimental results were compared for the CFD models' validation purposes. This process was repeated until the simulation and experimental results matched so that the numerical simulation results could be exported.

2.1. Combustion Chamber Geometry and Computational Mesh

The object of this study is a 2-stroke heavy-duty ME-GI DF marine engine. This is a DF engine that operates according to the diesel cycle. The engine can be operated smoothly in both diesel and DF modes. In the diesel mode, the engine works with diesel oil only. In the DF mode, diesel oil serves only as a pilot fuel to provide an ignition source, while NG serves as a primary fuel. In ME-GI engines, both the gaseous primary and liquid pilot fuels are directly injected into the engine cylinder by gas and pilot nozzles accordingly. In this study, the effects of SA and IP on the cylinder pressure, temperature, performance, and emission characteristics of the engine in both diesel and DF modes were analyzed.

The CFD analysis is derived from the finite volume method (FVM). This method reduces the degrees of freedom (DoF) from infinite to finite with the help of discretization or meshing. In CFD analysis, a continuous fluid domain is divided into a discrete domain consisting of a finite number of elements called "elements", which are connected through "nodes". The governing equations of fluid dynamics (the continuity, momentum, and energy equations) in the computational domain will be calculated at these nodes. This means that the number of equations that need to be solved and thus the calculation time will be proportional to the number of nodes in the computational domain. Therefore, in most cases of CFD analysis, researchers will always try to reduce the number of nodes of the computational domain to be as low as possible while still ensuring the mesh quality criterion. For 3D computational domains that are symmetric (axis or plane), an effective way to reduce the number of nodes is to compute for only one symmetric part of the entire domain. The cutting surfaces of the computational domain will be assigned a "cyclic" or "periodic" boundary condition [33].

In ICE simulations, if the engine has an axis-symmetric combustion chamber, as typically found in CIE engines since they do not contain a spark plug geometry, it is highly recommended to use only one portion of the entire computational domain for simulation [34]. In this study, the engine uses 3 gas injectors for NG injection and 3 other pilot injectors for pilot fuel injection, spaced by 120 degrees evenly on the cylinder head. The piston surface is a U-type shape. Due to the axial symmetry of the engine, only a one-third section of the entire 3D model of the engine has been modeled in order to reduce the calculation time. The one-third section of the engine combustion chamber geometry is shown in Figure 1, while Table 1 shows the main specifications of the engine.
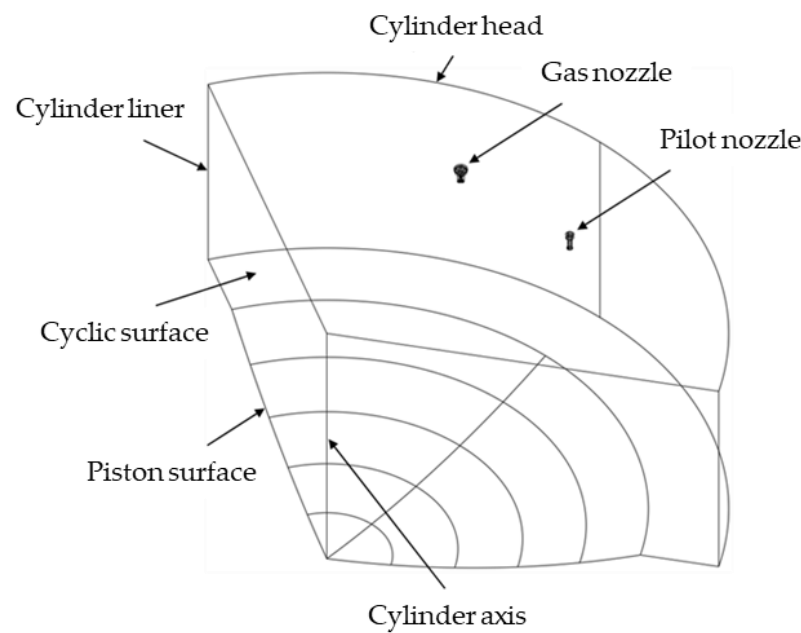
Figure 1. One-third portion of the engine combustion chamber geometry.

Table 1. Specifications of the simulated engine.

| Parameter	Value	Unit
Name of Engine	5G70ME-C9.5-GI	
Type of Engine	2-Stroke Dual-Fuel Engine	
Pilot Fuel Supplying Method	Direct Injection	
Gas Fuel Supplying Method	Direct Injection	
No. of Pilot Injector	3	
No. of Gas Injector	3	
No. of Cylinder	5	
Cylinder Bore x Stroke	700 × 3256	mm
Compression Ratio	13.7	-
Connecting Rod Length	4075	mm
Rated Speed	70	rpm
Rated Power @ Rated Speed	10,225	kW
Indicated Mean Effective Pressure (IMEP)	15.8	bar

Figure 2 shows the one-third portion of the entire 3D computational mesh of the combustion chamber at the top dead center (TDC) of the engine. The movement of the piston surface during the calculation was modeled by a dynamic mesh generated by the layering method. Due to the characteristics of the layering method, the computational mesh used in this study is a structured mesh with all elements in the computational domain as hexahedral cells. The movement of the piston surface was controlled by Equation (1). The mesh properties together with mesh quality are shown in Table 2.

$$P_l = \sqrt{(r_c + L)^2 - x_{offset}^2} - r_c \cos(\theta_c) - \sqrt{L^2 - (r_c \sin(\theta_c) + x_{offset})^2} \tag{1}$$

where P_l is the piston location, r_c is the crank radius, L is the length of the connecting rod, x_{offset} is the piston pin offset, while θ_c is the current crank angle degree (CAD).

In this study, the computational mesh is re-meshed according to the movement of the piston based on the dynamic Layering method. During the piston movement, mesh layers will be added or collapsed depending on the movement direction of the piston (downward or upward movement). This means that the number of mesh layers and thus the number of elements will be increased or decreased according to the moving down or up of the

piston. In this way, the mesh quality and resolution will be kept almost unchanged during calculation. In this moving action of the piston, only the cylinder liner surface and interior of the computational mesh were re-meshed by the Layering method. The cylinder head surface stayed stable.
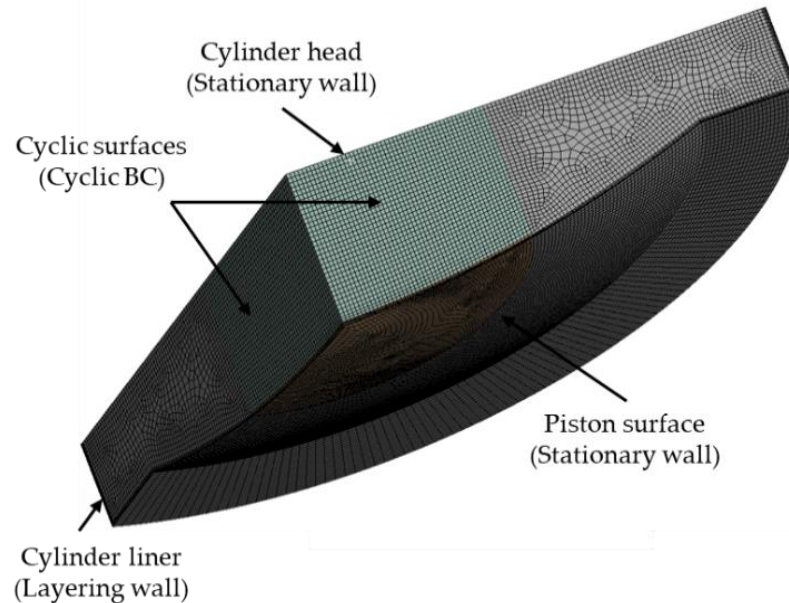
Figure 2. One-third portion of the 3D computational mesh of the engine combustion chamber at the TDC.

**Table 2.** Mesh properties and qualities.

Mesh Properties and Qualities	
Type of elements	Hexahedral
No. of nodes at the TDC	63,903
No. of elements at the TDC	66,715
Inflation	Total Thickness
Maximum thickness [mm]	1.2
Number of layers [-]	5
Growth rate [-]	1.2
Maximum aspect ratio [-]	17.07
Maximum skewness ratio [-]	0.78
Minimum orthogonal quality [-]	0.55

In this study, the Stochastic Collision model was used to model the interaction between the fuel droplets and combustion chamber walls. To eliminate the near-wall effects of the piston and cylinder liner surfaces, an inflation with 1.2 mm thickness and 5 inflation layers was applied on the piston and cylinder liner surfaces. Since the target point of fuel injection is only forwards toward the piston and cylinder liner surfaces of the engine, the effects of the near-wall behavior of the cylinder head surface can be neglected. The inflation option therefore only needs to be applied to the piston and cylinder liner surfaces.

2.2. Simulation Cases and Fuel Properties

Eighteen simulations have been carried out for both diesel and DF modes. Specifically, in each operating mode (diesel and DF mode), the IP has been adjusted to 0.01 m, 0.015 m, and 0.02 m distance from the cylinder head surface; in each IP, the SA was adjusted to angles of 40, 45, 50 degrees relative to the vertical direction. Figure 3 shows the schematic of the SA and IP adjustment in this study. Table 3 presents the simulation cases for each operating mode. The simulation results were then compared to determine the optimal

parameters for the fuel injector, i.e., the SA and IP of the nozzle. In this study, CH_4 was used to represent NG, while $C_{10}H_{22}$ was used to represent diesel oil. The main properties of CH_4 and $C_{10}H_{22}$ are shown in Table 4.
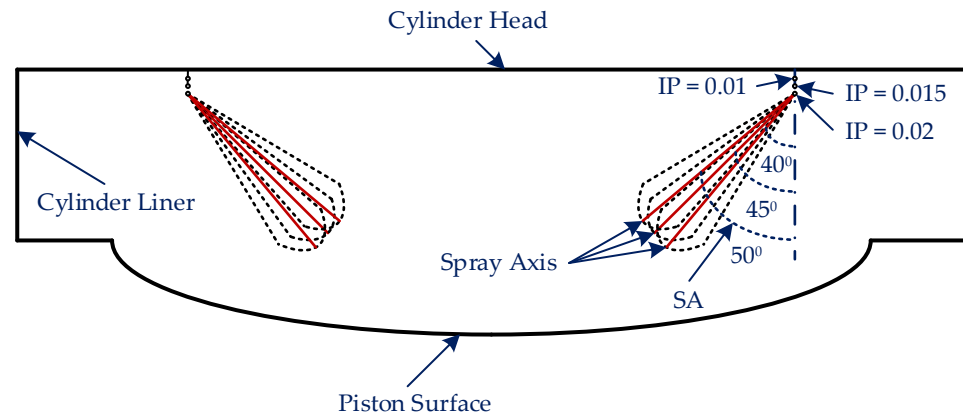
Figure 3. Schematic of the SA and IP adjustments.

Table 3. Summary of the simulation cases.

Simulation Case		Injection Position (IP) [Unit: m]		
		0.01	**0.015**	**0.02**
Spray Angle (SA) [Unit: degree]	40	SA = 40/IP = 0.01	SA = 40/IP = 0.015	SA = 40/IP = 0.02
	45	SA = 45/IP = 0.01	SA = 45/IP = 0.015	SA = 45/IP = 0.02
	50	SA = 50/IP = 0.01	SA = 50/IP = 0.015	SA = 50/IP = 0.02

Table 4. Fuel properties [33,35,36].

Fuel	Diesel	NG	Unit
Density	730	0.657	kg/m^3 @ 25 °C, 1 at
Chemical name/formula	n-Decane/$C_{10}H_{22}$	Methane/CH_4	
Lower calorific value	42,000	50,000	kJ/kg
Molecular weight	142.284	16.043	g/mol
Boiling point	174	−162	°C
Auto-ignition temperature	223	537	°C
Specific heat capacity (Cp)	2090	35.69	J/mol·K @ 25 °C
Stoichiometric air–fuel ratio	14.98	17.19	kg/kg

2.3. CFD Models and Governing Equations

This study used the pressure-based type with absolute velocity formation for the solver. The effect of gravitational acceleration was also included in the simulation. The acceleration value used was 9.81 m/s^2. Due to the piston's moving action during the simulation, an unsteady (transient) approach was used. In engine modeling, the time step size is calculated based on the piston movement speed. The time step size value was 4.62963×10^{-5} s. However, due to the complexity of the fuel combustion process, the time step size of the simulation during this period (12 CADs BTDC to 20 CADs ATDC) was set to be reduced to 16 times to ensure solution convergence. Here, 50 maximum iterations per time step were set. Monitoring the residuals showed that the solution reached convergence after 31 to 35 iterations per time step, and the computation was then skipped to the next time step. The PISO scheme with a value of 1 for both skewness and neighbor corrections was applied. For spatial discretization, the Green-Gauss Node-Based gradient and standard pressure were used. Meanwhile, Second-Order Upwind was applied for density, momentum, TKE, turbulent dissipation rate, nuclei, and pollutant calculations. An

absolute criterion of 10^{-3} for convergence criteria was set for continuity, velocity, k, and ε, while a stricter criterion of 10^{-6} was set for energy and pollutant calculations. These convergence criteria are suitable for combustion and emission simulations of internal combustion engines, as presented in [33].

The standard k-ε turbulence model was employed to model the fluid flow turbulence inside the engine cylinder. This model is suitable and widely used to model the turbulence inside the cylinder of ICEs [37]. The combustion of fuel in the engine cylinder was modeled by the non-premixed combustion model using a reduced chemical mechanism. The reduced chemical reaction was generated using the probability density function (PDF) method in the ANSYS Fluent solver. This model is suitable for simulating non-premixed combustion, where the oxidizers and fuels are introduced into the combustion apparatus separately [33]. Reaction mechanisms play a very important role in combustion simulations. For a deeper understanding of the reaction mechanism as well as the latest developments in this field, it would be helpful to refer to [38]. To simulate the spraying of the nozzle, the Discrete Phase Model (DPM) was used. This model offers an effective way to correct the spray velocities and initial droplet diameters caused by the cavitation phenomenon. In this model, the Kelvin–Helmholtz Rayleigh–Taylor (KHRT) sub-model was utilized to model the breakup phenomenon of fuel droplets. Meanwhile, the auto-ignition model was employed to simulate the self-ignition of fuel in the engine cylinder.

The composition PDF transport governing equation is derived from the Navier–Stokes equations as [39]:

$$\frac{\partial}{\partial t}(\rho P) + \frac{\partial}{\partial x_i}(\rho u_i P) + \frac{\partial}{\partial \psi_k}(\rho S_k P) = -\frac{\partial}{\partial x_i}\left[\rho \langle u_i'' | \psi \rangle P\right] + \frac{\partial}{\partial \psi_k}\left[\rho \left\langle \frac{1}{\rho}\frac{\partial J_{i,k}}{\partial x_i}\middle| \psi \right\rangle P\right] \quad (2)$$

where,

$\rho =$	mean fluid density;
$P =$	Favre joint PDF of composition;
$u_i =$	Favre mean fluid velocity vector;
$\psi =$	composition space vector;
$S_k =$	reaction rate for specie k;
$J_{i,k} =$	molecular diffusion flux vector;
$u_i'' =$	fluid velocity fluctuation vector.

In Equation (2), the notation $\langle \ldots \rangle$ denotes expectations, while $\langle A|B \rangle$ is the conditional probability of event A, given that event B occurs. Meanwhile, the two terms on the right-hand side of the equation represent the PDF change due to scalar convection caused by turbulence (turbulent scalar flux) and molecular mixing/diffusion, respectively.

The turbulent scalar flux term is modeled by the gradient-diffusion assumption:

$$-\frac{\partial}{\partial x_i}\left[\rho \langle u_i'' | \psi \rangle P\right] = \frac{\partial}{\partial x_i}\left(\frac{\rho \mu_t}{Sc_t}\frac{\partial P}{\partial x_i}\right) \quad (3)$$

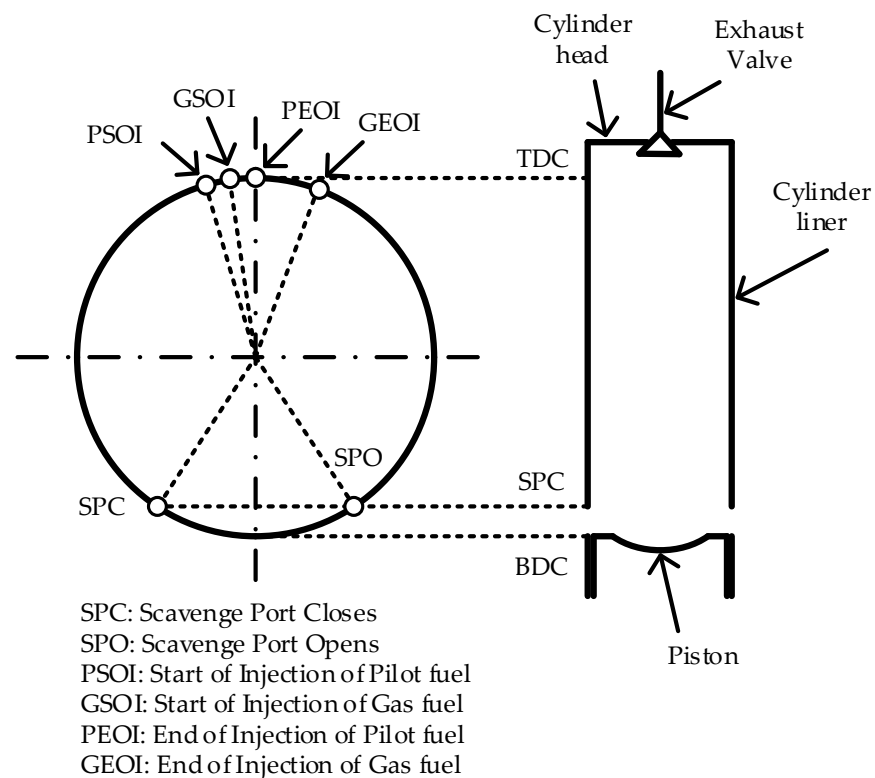where μ_t and Sc_t are the turbulent viscosity and Schmidt number, respectively.

The Extended Zeldovich mechanism was utilized to model the NO formation occurring inside the engine cylinder [33,40]. This reaction mechanism consists of 7 species and 3 chemical reactions and can highly accurately predict NO formation over a wide equivalence ratio range. This model is presented in Appendix A of this article and can also be referenced in detail in our previous publications [11,12,21]. The soot formation during the combustion process of the engine was modeled by the Moss–Brookes model [33,41,42]. The collisions and interactions between the injected fuel droplets and combustion chamber walls were modeled using the Stochastic Collision sub-model. This model is derived from the O'Rourke algorithm [33,41,42]. The CFD models used in this study have been successfully applied and can be found in our previous publication [21] or references [33,40,41]. Table 5 shows a summary of the CFD numerical models used in this study.

Table 5. Summary of the CFD models.

Model	Description	
Combustion	Non-premixed combustion model coupling with the PDF reduced chemical mechanism	
Emission	NO	Extended Zeldovich
	Soot	Moss–Brookes model
Fuel injection	Spray	Discrete Phase Model (DPM)
	Breakup	KHRT
	Ignition	Auto-ignition
Collision	Stochastic Collision model	
Turbulence	Standard k-ε model	

2.4. Boundary and Initial Conditions

The boundary conditions (BCs) at the cylinder liner, cylinder head, and piston surface were defined as impermeable walls. The geometry of the combustion chamber is axially symmetric, so the cutting surfaces of the cutting portion of the computational domain were assigned as cyclic BCs. The simulation was started from the SPC of 30 crank angle degrees (CADs) after the bottom dead center (BDC) to the EVO of 30 CADs before the bottom dead center (BBDC) of the engine. The start of injection (SOI) of the pilot and gaseous fuels were 12 and 10 CAD BTDC, respectively. The injection duration of the pilot and gaseous fuels were 12 and 30 CADs, respectively. The single-injection method with step impulse function was applied for both pilot and gas fuel injections. The injection processes take place from the SOI to the EOI continuously with constant mass flow rates. A schematic of the working process of the engine is shown in Figure 4. The BC$_S$ and initial conditions for the numerical CFD simulations in this study were obtained from the engine shop test experiments and are summarized in Table 6.

SPC: Scavenge Port Closes
SPO: Scavenge Port Opens
PSOI: Start of Injection of Pilot fuel
GSOI: Start of Injection of Gas fuel
PEOI: End of Injection of Pilot fuel
GEOI: End of Injection of Gas fuel

Figure 4. Schematic of the working process of the engine.

**Table 6.** Boundary and initial conditions for the CFD numerical simulations.

Boundary Names	Boundary Types	Specific Conditions/Values
Piston	Movable wall	Temp./297 °C
Liner	Layering wall	Temp./197 °C
Cylinder head	Stationary wall	Temp./297 °C
Segment cut	Cyclic	

Initial Conditions		Values
Scavenging air temp.		46 °C
Scavenging air press.		2.2 Bar
SPC		30 CAD ABDC
EVO		30 CAD BBDC
Start of injection (SOI)	Pilot fuel	12 CAD BTDC
	Gaseous fuel	10 CAD BTDC
End of injection (EOI)	Pilot fuel	TDC
	Gaseous fuel	20 CAD ATDC

2.5. Mesh Independence Analysis

Mesh density or mesh resolution plays an important role in mesh quality and therefore in the accuracy of the final CFD result. Additionally, mesh density also affects the calculation time. Therefore, to ensure the accuracy of the final CFD result and the reasonableness of the computation time, a mesh independence analysis was performed. Three simulations using three various mesh densities, including coarse, medium, and fine meshes, were performed to analyze the mesh independence of the solution. The simulations were performed in parallel using an Intel(R) Xeon(R) CPU X5690 @ 3.47 GHz, 16-core, 32-thread processor, 32 GB RAM Windows workstation. Table 7 shows the properties of the meshes with the respective calculation time in the mesh independence analysis. A comparison between the final CFD results using these three mesh densities is shown in Figure 5.

**Table 7.** Mesh properties and calculation time.

Mesh Metrics		Coarse	Medium	Fine
No. of Nodes at the BDC		908,868	1,204,763	1,692,454
No. of Elements at the BDC		875,672	1,164,920	1,642,512
Quality	Max. Aspect Ratio	26.295	26.161	23.472
	Max. Skewness	0.609	0.652	0.623
	Min. Orthogonal	0.599	0.529	0.484
Calculation Time		48 h	60 h	84 h
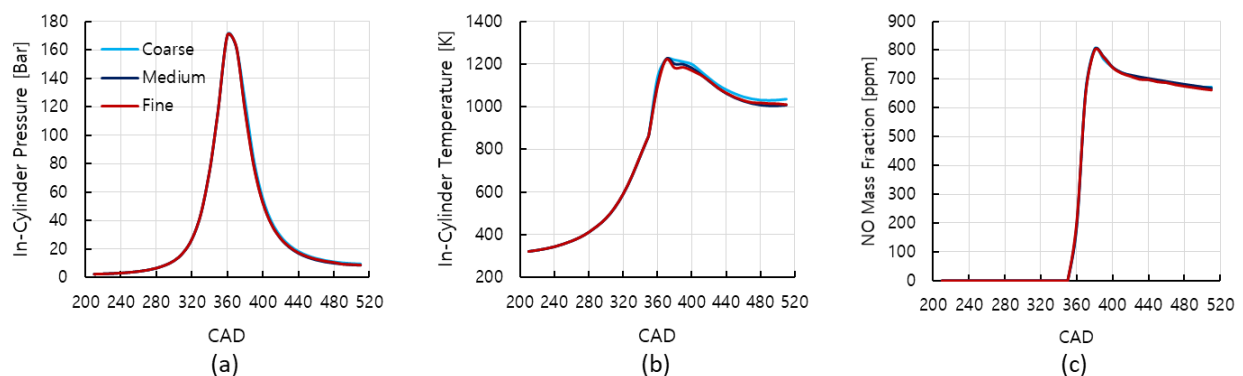
Figure 5. Comparison of the simulation results among various mesh densities: (**a**) In-Cylinder pressure; (**b**) In-Cylinder temperature; (**c**) NO mass fraction.

The comparison showed the good agreement of the final CFD results between the medium and fine mesh cases. Therefore, the medium mesh was chosen for simulations in this study because it gave accurate CFD results that were the same as the fine mesh but in a shorter calculation time.

2.6. CFD Model Validation

The CFD models used in this study have been validated by comparing the numerical simulation results to the experimental results reported in the engine's shop test data. The comparisons between the simulation and experimental results for both diesel and DF modes are shown in Figure 6. The variables used for the CFD models' validation are in-cylinder peak pressure (Figure 6a), indicated mean efficiency pressure (IMEP) (Figure 6b), and NO emission (Figure 6c). It is obvious that the numerical simulation results and experimental results are in good agreement. The maximum deviation between the simulation and experimental results was only 7% in the case of NO emission comparison in the diesel mode. Meanwhile, the deviations between the remaining cases were less than 1%. These deviations are within the 10% limitation, which is widely accepted in CFD analysis [43,44]. The validated CFD models were then utilized for numerical simulations when adjusting the SA and IP of the fuel nozzle in this study.
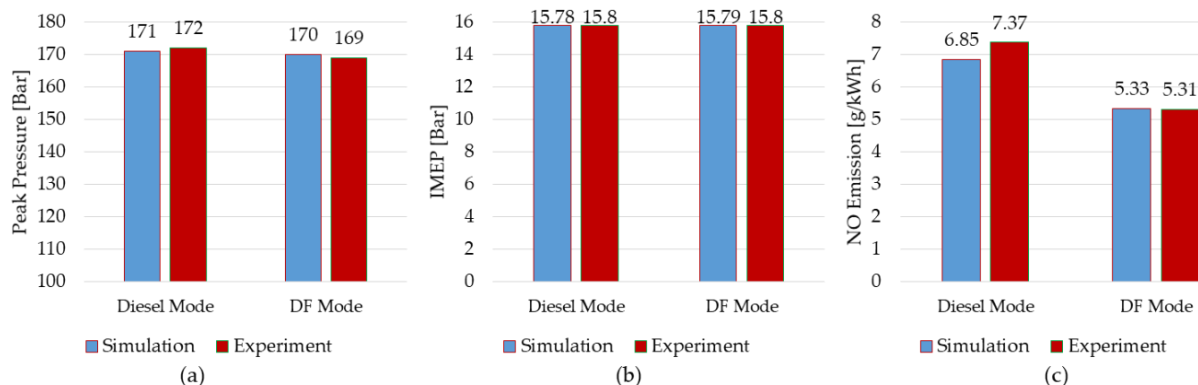
Figure 6. Comparison between the simulation and experimental results: (**a**) Peak pressure; (**b**) IMEP; (**c**) NO emission.

The model validation demonstrated that the right models were selected among the CFD models for the simulation of the engine. Therefore, these models can in principle be applied to simulate the same phenomena occurring in similar types of engines (i.e., gas–diesel DF engines using the direct-injection method for fuel introduction). In fact, the accuracy of a CFD simulation result depends not only on the models chosen but also on the quality of the mesh. Therefore, when applying these validated models in this study to simulate similar phenomena in similar types of engines, performing a mesh independence analysis of the CFD results is necessary. This was to ensure the suitability of the chosen CFD models for another geometry. To perform a mesh independence analysis, it is recommended to refer to the procedure suggested by Celik [45].

3. Results

To clarify the effects of SA and IP on the combustion and emissions of the engine, only these two parameters were adjusted during the simulation setup. Other simulation parameters were kept the same.

3.1. Velocity Vectors and Turbulence Kinetic Energies

Figure 7 shows the velocity vectors in the cylinder on the central plane at the TDC of the engine. The simulation results showed that the velocity inside the engine cylinder reached the maximum value at the SA of 45 degrees in all three IP cases (IP = 0.01, 0.015, and 0.02 mm) in both diesel and DF modes. This tendency can be explained by the fact

that since the environment inside the cylinder is the same in all cases, the velocity of the injected fuel will be affected only by SA and IP. SA and IP specify the direction and the target region of the injection in the engine cylinder. The direction and the target region of the injection are very important because they affect the interaction between fuel injection streamlines from radial nozzles in this engine, as well as between fuel injection streamlines and the piston surface. When the SA was 40 degrees, the target region of the injection became closer to the piston surface. Meanwhile, when the SA was 50 degrees, the target regions of radial injections interacted with each other. Higher interactions among radial injections and between the injected fuel and piston surface led to a reduction in the fuel velocity inside the engine cylinder. These interactions can be observed in Figure 7.
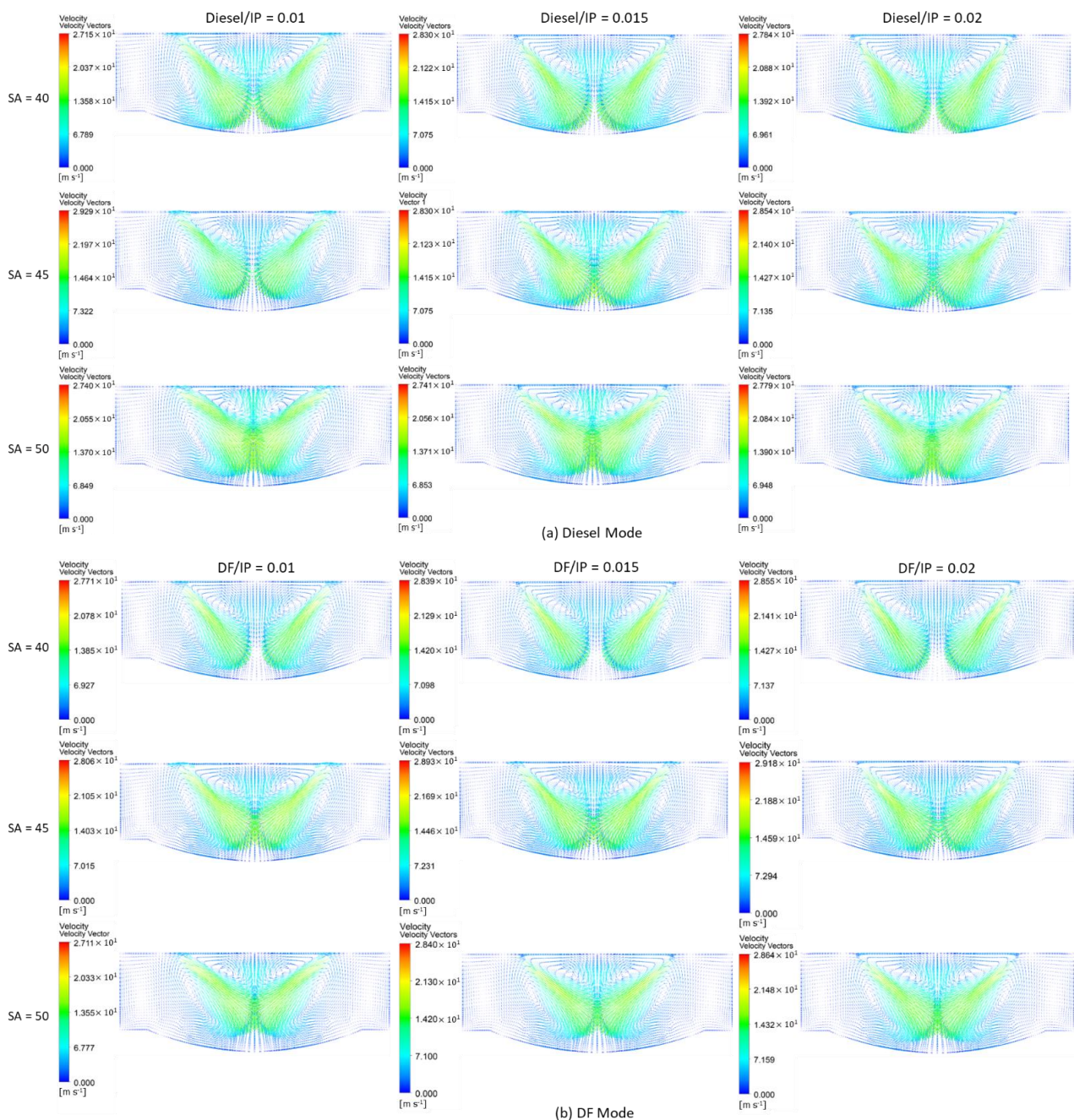
Figure 7. Velocity vectors in the engine cylinder at the TDC in all simulation cases with various SA and IP: (**a**) Diesel modes, (**b**) DF modes.

Figure 8 shows the TKEs in the engine cylinder in all simulation cases. It can be observed from the figure that the TKEs in the diesel modes were higher than those in the DF modes at each SA in all three IP cases. Moreover, in both diesel and DF modes, TKE tended to increase as SA decreased from 50 to 40 degrees. As is known, in fluid dynamics, TKE is the average kinetic energy in one unit of mass associated with vortexes in turbulent flows. Physically, TKE is characterized by the fluctuations of the measured root-mean-square (RMS) velocities. Generally, TKE is defined as half the sum of the fluid flow velocity component variances (square of standard deviations), as expressed in Equation (4) [46].

$$k = \frac{1}{2}\left(\overline{(uı)^2} + \overline{(vı)^2} + \overline{(\omega ı)^2}\right) \tag{4}$$

where, k, $uı$, $vı$, and $\omega ı$ are the TKE and the velocity components according to the horizontal (x- and y-axis) and vertical (z-axis) directions of vortexes in turbulence flows, respectively. As can be seen, TKE is proportional to the square of the turbulence velocity components of fluid flows. In other words, TKE indicates the turbulence intensity of fluid flows.
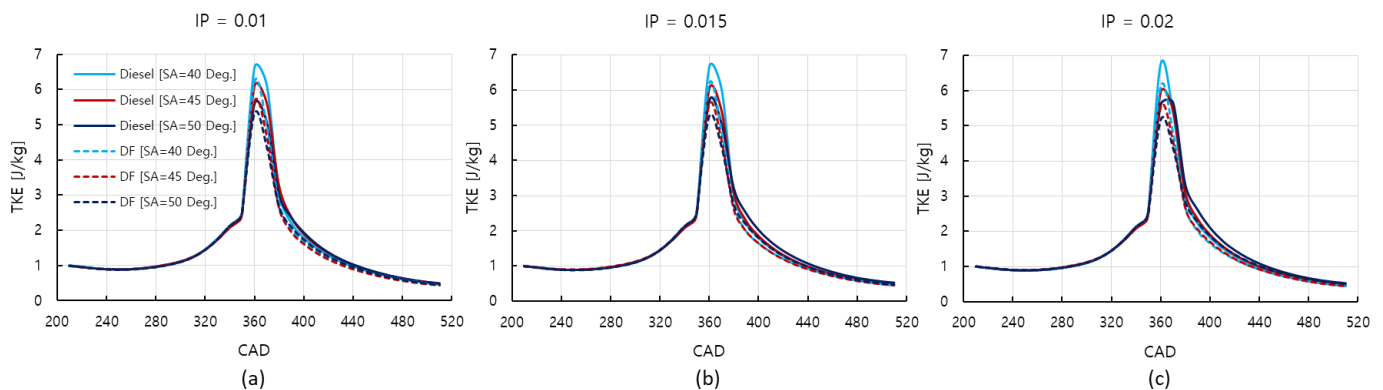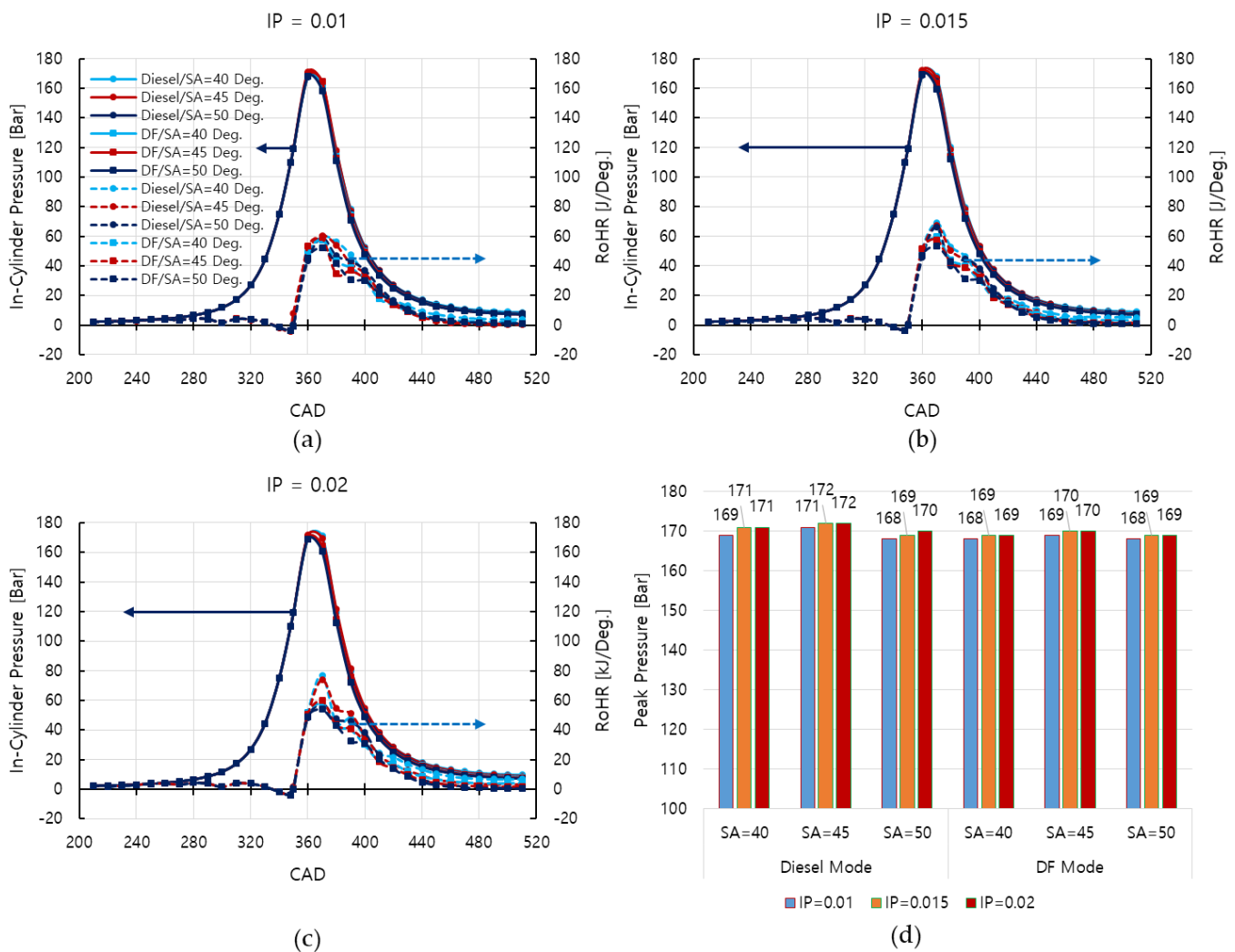

Figure 8. TKEs in the engine cylinder in all simulation cases: (**a**) IP = 0.001 m; (**b**) IP = 0.015 m; (**c**) IP = 0.02 m.

In this study, when the SA was reduced from 50 to 40 degrees, the target region of injection shifted closer to the piston surface. Since the piston surface was U-shaped, the target injection region closer to the piston surface led to increases in the vortex intensity of the fluid flow. As a result, the increase in vortex intensity led to an increase in the TKEs in all three IP cases in both diesel and DF modes, as shown in Figure 8. In addition, in each SA case, the increase in IP from 0.01 to 0.02 m also shifted the target injection regions closer to the piston surface. Both the increase in TKE and the target injection region shifting closer to the piston surface will affect the soot formation of the engine. This will be analyzed in detail in Section 3.4.

3.2. In-Cylinder Pressure and Engine Performance

Figure 9 shows the effect of SA and IP on the in-cylinder pressure of the engine. Figure 9a–c present the pressures and RoHRs inside the engine cylinder with various SAs in the 0.01, 0.015, and 0.02 m IP cases, respectively. Meanwhile, Figure 9d shows a summary of the in-cylinder peak pressure in all simulation cases.

Although the difference in peak pressure among simulation cases was not significant, it can be observed that the peak pressure tended to increase slightly as IP increased at each SA in both diesel and DF modes. Among SA cases, the SA of 45 degrees produced the highest in-cylinder peak pressure in both diesel and DF modes. Considering the effects of both SA and IP on the in-cylinder pressure, Figure 9d shows that the SA of 45 degrees with an IP of 0.015 or 0.02 m produced the highest peak pressure in both diesel and DF modes.

Figure 9. In-cylinder pressure and RoHR diagrams in the IP = 0.01 m case (**a**), IP = 0.015 m case (**b**), IP = 0.02 m case (**c**), and peak pressure in all cases (**d**).

Figure 10 shows the Indicated Mean Effective Pressure (IMEP) of the engine in all simulation cases. The simulation results showed an increasing tendency in the IMEP of the engine as the IP increased in both diesel and DF modes. Meanwhile, it tended to decrease as SA increased from 40 to 50 degrees. Among these cases, an IP of 0.02 m with an SA of 40 degrees produced the highest IMEP for the engine in both diesel and DF modes. Specifically, this set of injection parameters increased the IMEP of the engine by 11.15% and 6.08% compared to when using the original set of injection parameters (IP = 0.01/SA = 45) in the diesel and DF mode, respectively. It is thus considered to be the optimal parameter that should be set for the fuel injector to enhance engine performance in both diesel and DF modes. The fact that the engine reached the highest performance with this set of injection parameters might be because the target injection region of the injector was in the optimal combustion region of the engine in this case.

3.3. In-Cylinder Temperature and NO Emission

The temperature distributions inside the engine cylinder at the TDC in all simulation cases are shown in Figure 11. From the figure, it is very easy to observe and visualize the effect of SA and IP on the target injection region mentioned in Section 3.1. This figure helps the readers to observe and visualize more clearly the positional relationship between the radial fuel injection regions, as well as between the fuel injection regions and the piston

surface when adjusting the SA and IP in this study. Figure 11 also clearly shows regions of high temperature (≥1800 K—red color regions) where NOx is normally formed.
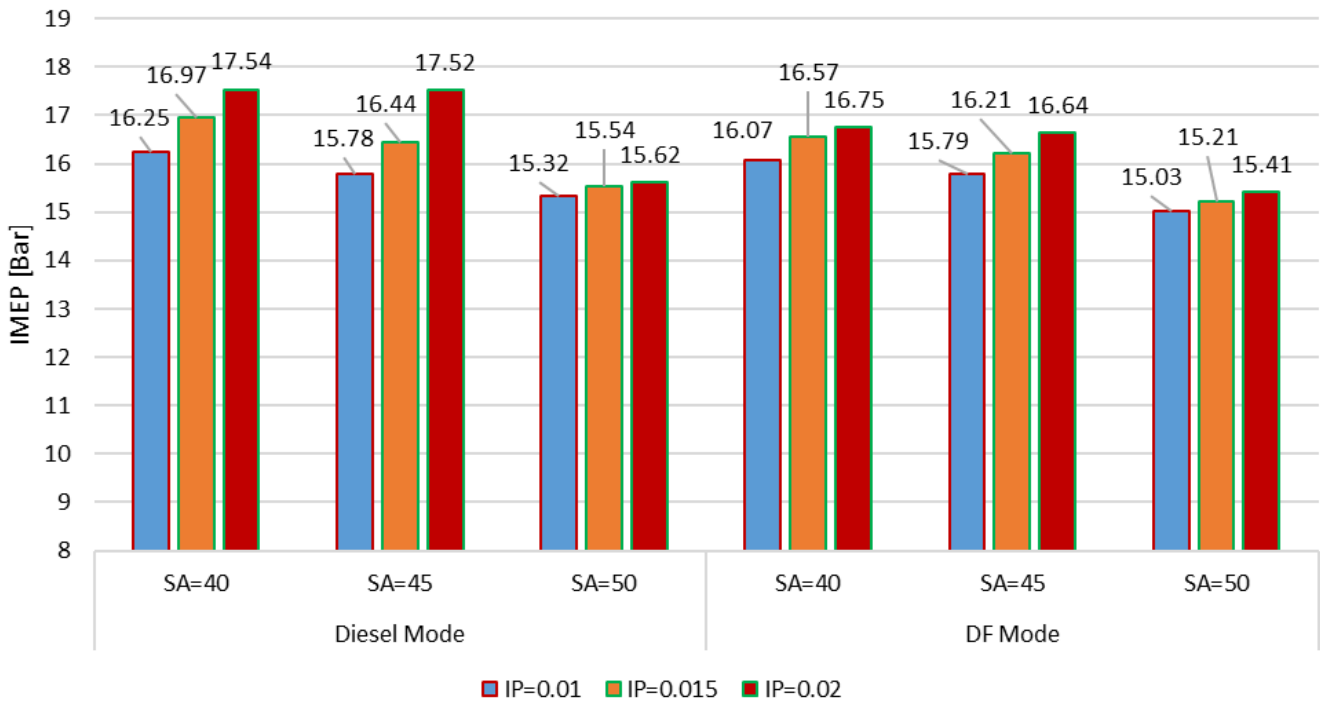

Figure 10. IMEPs of the engine in all simulation cases.
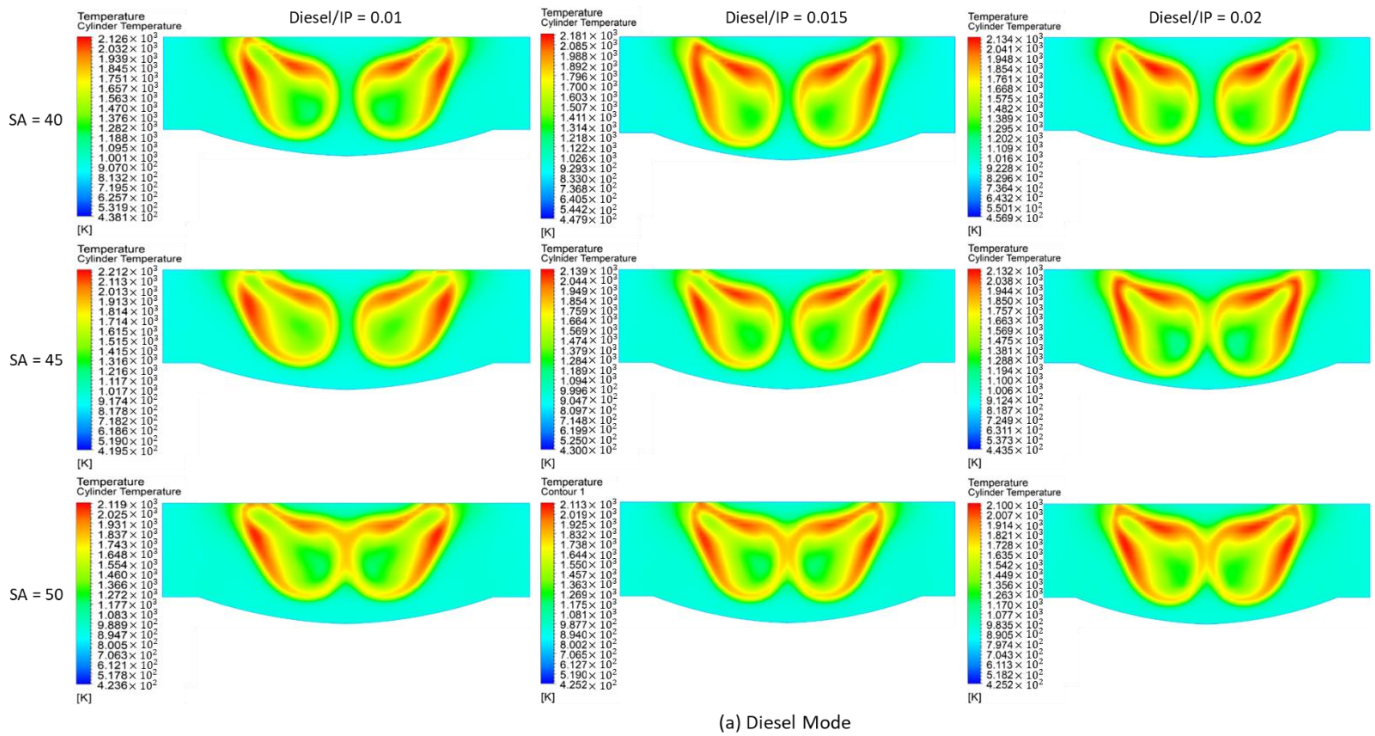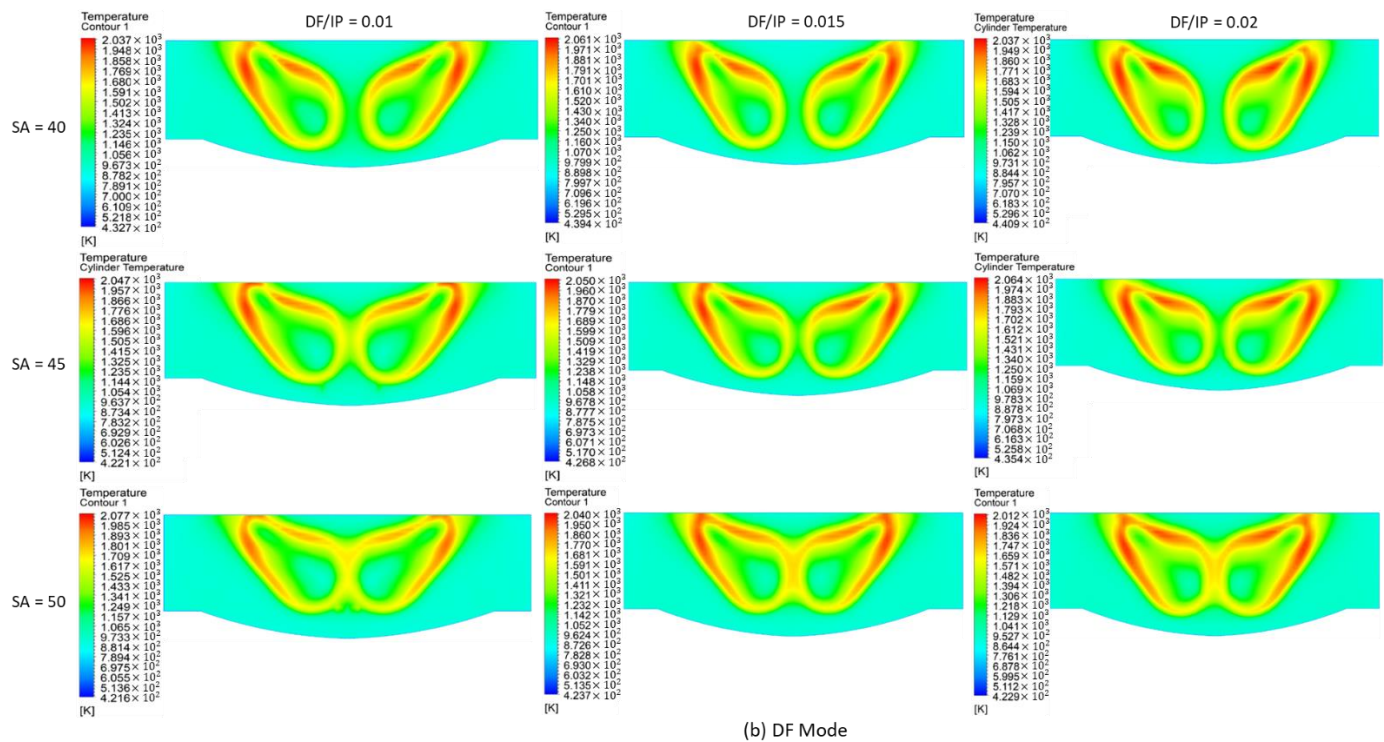


(a) Diesel Mode

Figure 11. *Cont.*

Figure 11. Temperature distributions inside the engine cylinder at the TDC in all simulation cases: (**a**) Diesel mode, (**b**) DF modes.

Figure 12 shows the in-cylinder temperature diagrams, while Figure 13 shows a summary of the in-cylinder peak average temperatures in all simulation cases. The simulation results showed a lower peak temperature in the DF modes compared to the diesel modes. Moreover, the in-cylinder temperature during the expansion process of the engine in the DF modes was lower than that compared to the diesel modes. The lower cylinder temperature in the DF mode compared to the diesel mode may be due to the more homogeneous quality of the fuel–air mixture within the engine combustion chamber in the DF mode. As is known, the viscosity and molecular size of gaseous fuels are many times smaller than those of liquid fuel droplets. Therefore, when injected into engine cylinders, the quality of mixing with the air in the engine cylinders of gaseous fuels is also better than that of liquid fuels. The higher homogeneous quality within the engine combustion chamber helped to distribute the temperature from the combustion throughout the engine cylinder more uniformly. As a result, this consequently resulted in a reduction in both the peak temperature and in-cylinder temperature during the expansion process in the DF mode compared to those in the diesel mode, as shown in Figures 12 and 13.

At each SA, the simulation results showed an increasing tendency in peak temperature as the IP increased in both diesel and DF modes. As mentioned above, as the IP increased, the target injection region shifted closer to the piston surface. Due to the U-shaped piston surface, the displacement of the target injection region closer to the piston surface may have increased the degree of swirl inside the engine combustion chamber. The increased vortex level increased the mixing quality of the air–fuel mixture, leading to an increase in the quality of combustion inside the engine combustion chamber. As a result, the peak temperature in the cylinder increased, as can be observed in Figure 13. Meanwhile, among SAs, the SA of 45 degrees produced the highest peak temperature in both diesel and DF modes.
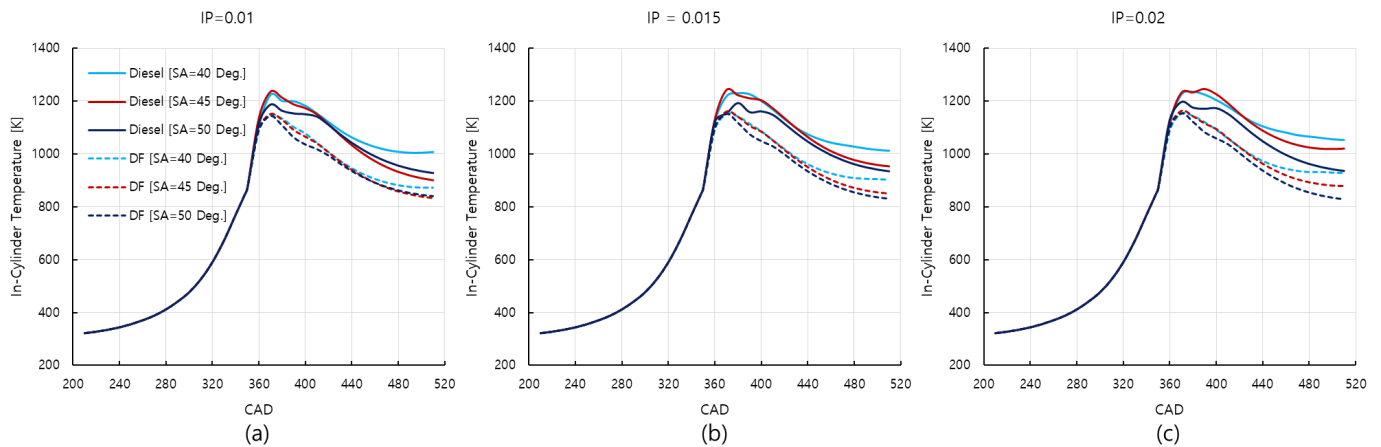
Figure 12. In-cylinder average temperature diagrams in all simulation cases: (**a**) IP = 0.01 m; (**b**) IP = 0.015 m; (**c**) IP = 0.02 m.
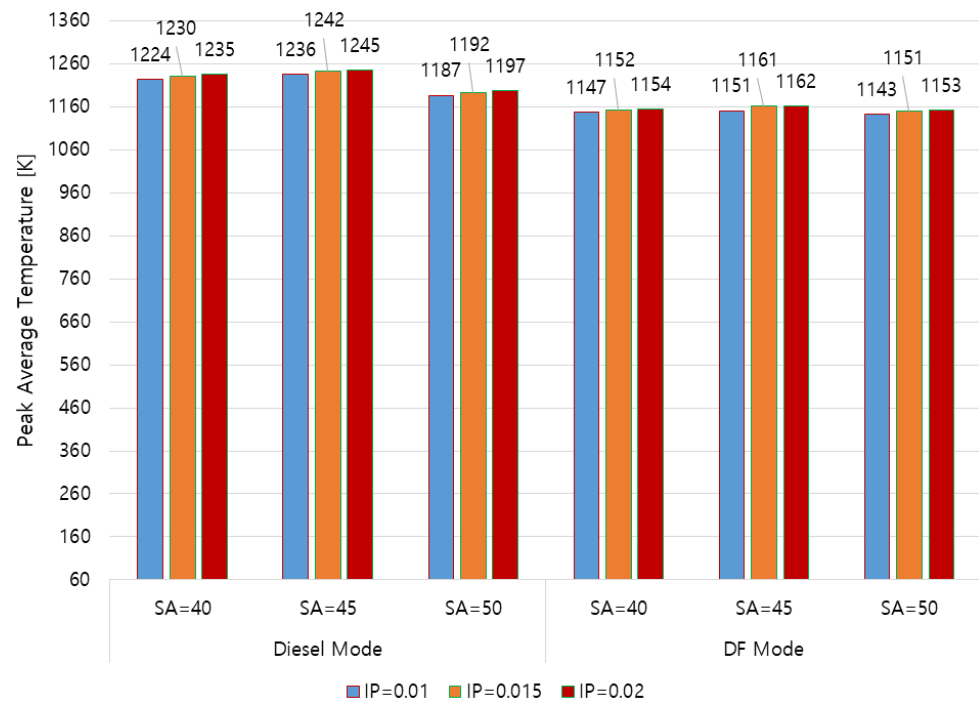
Figure 13. In-cylinder peak average temperatures in all simulation cases.

Additionally, as is widely known, for both ideal and real gases, under the same volumetric conditions, the pressure and temperature of gases are linearly proportional to each other. This explains why the changes in peak pressure and peak temperature in the engine cylinder according to the changes in SA and IP had the same trend, as can be compared between Figures 9d and 13.

Figure 14a,b show the NO mass fraction and specific NO emission in all simulation cases, respectively. Figure 14a shows that, at each SA, the NO mass fraction tended to increase as the IP increased. Meanwhile, among SAs, the SA of 45 degrees also produced the highest NO mass fraction with the same trend as in the in-cylinder peak temperature. In comparison to the diesel modes, the DF modes produced lower NO mass fractions due to the lower peak temperatures inside the engine cylinder. This trend was also reported in studies in [7,11,12].
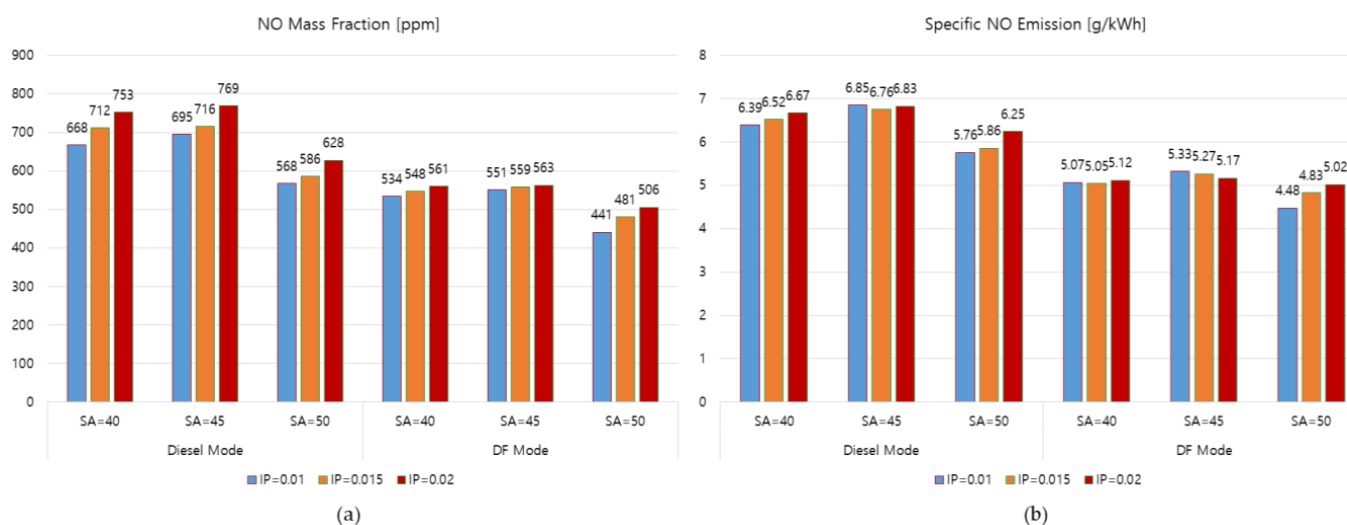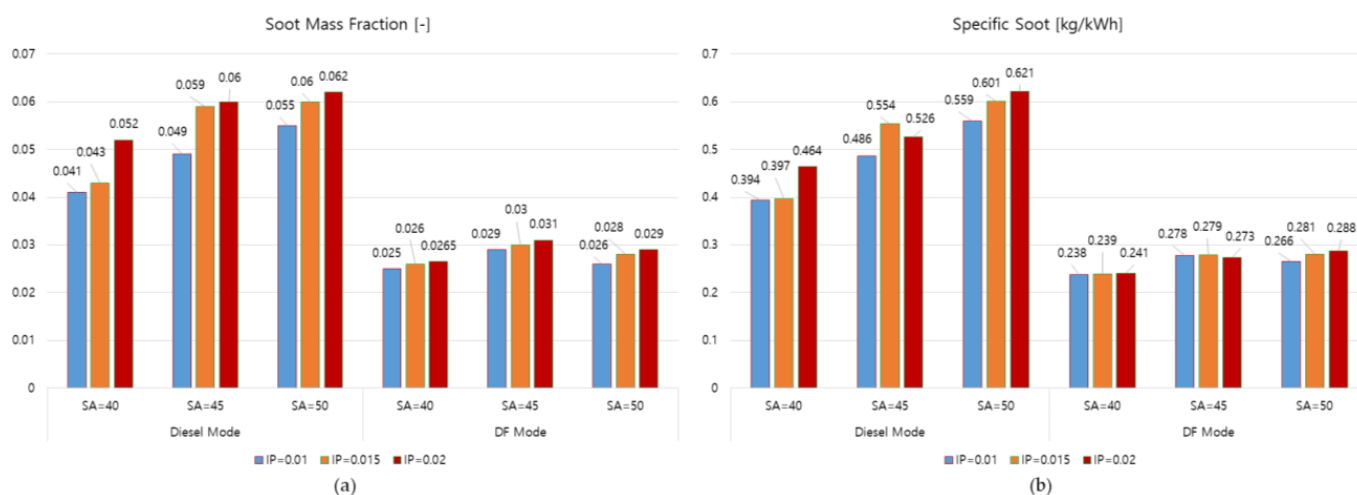
Figure 14. NO emissions in all simulation cases: (**a**) NO mass fraction, (**b**) specific NO emissions.

It is widely known that NO (nitric oxide) is the main component of NOx emissions generated from ICEs and usually occupies more than 90% of NOx. Three typical chemical mechanisms are involved in NOx formation: the thermal NOx mechanism, the prompt NOx mechanism, and the fuel NOx mechanism [47]. However, in ICEs that operate with nitrogen-free fuels, only the NOx thermal mechanism must be considered. This is why the Extended Zelodovich mechanism was used to model NO formation in this study. According to this mechanism, NO formation is mainly influenced by the in-cylinder peak temperature, the residual time, and the oxygen concentration inside the engine cylinder. NO formation occurs strongly in very high-temperature ($\geq$1800 K) regions in the cylinder, and the formation rate significantly increases according to the increase in the in-cylinder peak temperature [10,47]. Since NO formation is closely related to the peak temperature in the engine cylinder, it had the same trend as the peak temperature in the cylinder when the SA and IP varied. This can be verified by comparing Figures 13 and 14a.

However, when expressing the NO emission in terms of specific values (the amount of NO emission (gram) generated per unit time (1 h) per unit engine power (1 kilowatt)), the NO emission had a different trend, as shown in Figure 14b. It can be seen from Figure 14b that the IP of 0.01 m with an SA of 50 degrees produced the lowest specific NO emission in both diesel and DF modes. This set of injection parameters decreased the specific NO emissions of the engine by 18.92% and 18.97% compared to when using the original set of injection parameters (IP = 0.01/SA = 45) in the diesel and DF mode, respectively. It is thus considered to be the optimal parameter that should be set for the fuel injector to reduce NO emissions in both diesel and DF modes.

3.4. Soot Formation

The soot mass fraction and specific soot in all simulation cases are shown in Figures 14b and 15a, respectively. The simulation showed that the soot mass fraction tended to increase when the IP increased from 0.01 to 0.02 m at each SA in both diesel and DF modes. Meanwhile, at each IP, when the SA increased from 40 to 45 and 50 degrees, the soot mass fraction tended to increase in the diesel mode; it, however, tended to increase and then slightly decreased in the DF mode. These trends may be related to two main factors: (1) the intensity of turbulence inside the engine combustion chamber affected the local fuel–air equivalence ratio [6,47], and (2) the fuel films formed on the piston surface due to impinging sprays [6,48]. Under high fuel–air equivalence ratio (fuel-rich) conditions, which are typically found in the diffusion combustion of direct-injection CIEs, hydrocarbon fuels have a strong tendency to form carbonaceous particles, i.e., soot [49]. Meanwhile, the increase in fuel films formed on the piston surface increases soot formation.

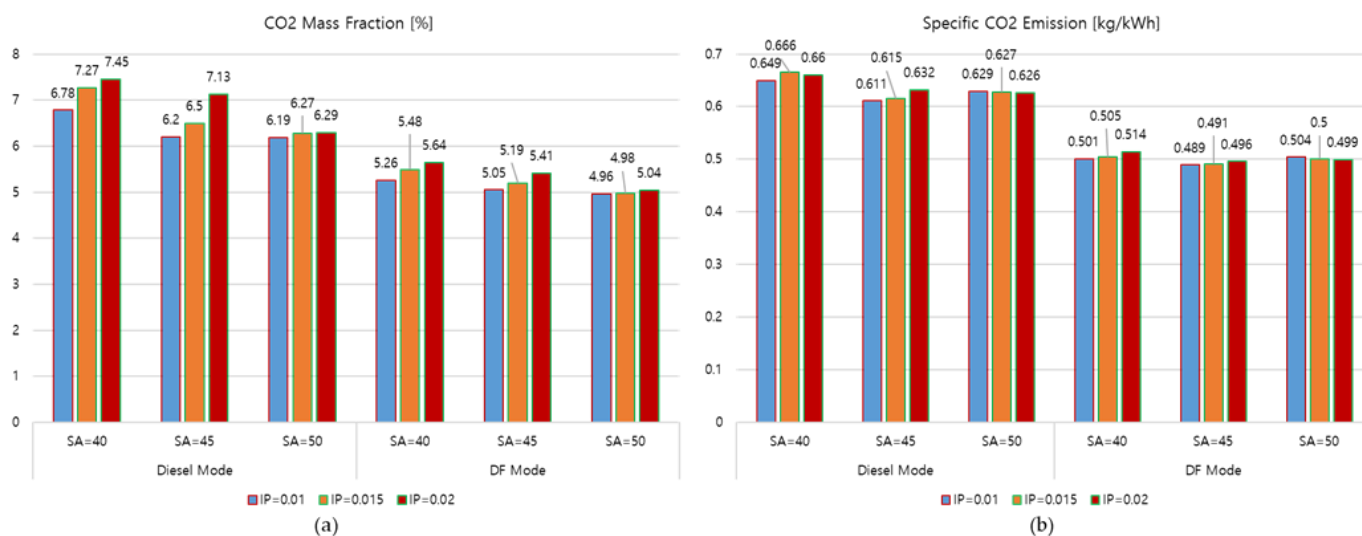**Figure 15.** Soot emissions in all simulation cases: (**a**) soot mass fraction, (**b**) specific soot.

In this study, soot formation tended to increase when the IP increased at each SA. This is due to the increase in fuel films formed on the piston surface caused by the target injection region of the fuel being shifted closer to the piston surface when the IP increased. This tendency can be observed in Figure 7 in Section 3.1 or Figure 11 in Section 3.3. Fang et al. also reported in [31] that the increase in the deposition of fuel film on the piston wall led to higher soot formation. The CFD simulation results obtained by Lim and Min [33] also showed higher soot formation due to injected fuel impingement onto the combustion chamber walls. Meanwhile, the increase in soot formation as the SA increased from 40 to 50 degrees at each IP may be related to higher local fuel–air equivalence ratios inside the engine combustion chamber. At each IP, the reductions in TKEs when the SA increased (Figure 8) reduced the mixing quality between the fuel and air. This led to increases in the local fuel–air equivalence ratio and thus increased soot formation.

Compared to the diesel modes, the DF modes produced significantly lower soot. This is because the mixing quality between the injected fuel and air in the DF modes (using gaseous fuel) was higher than that in the diesel mode (using liquid fuel). Higher fuel–air mixing quality resulted in significant reductions in the local fuel–air equivalence ratio in the DF modes. This helped to reduce soot formation in the DF mode. In addition, because CH_4 does not contain C-C bonds, and it contains no aromatics and sulfur, NG tends to minimally produce soot compared to other hydrocarbon fuels [1,50]. The reduction tendencies in soot formation in DF modes using CH_4 compared to the diesel mode using only diesel oil had also been reported in previous studies [10–12].

Considering engine power, when expressing the amount of soot emitted in terms of specific values, the simulation result showed a different trend, as can be seen in Figure 15b. It can be seen from the figure that the IP of 0.01 m with an SA of 40 degrees produced the lowest specific soot emission in both diesel and DF modes. This set of injection parameters decreased the specific soot emissions of the engine by 23.35% and 16.81% compared to when using the original set of injection parameters (IP = 0.01/SA = 45) in the diesel and DF mode, respectively. It is thus considered to be the optimal parameter that should be set for the fuel injector to reduce soot emissions in both diesel and DF modes.

3.5. Carbon Dioxide (CO_2) Emission

Figure 16a,b show the CO_2 mass fractions and specific CO_2 emissions in all simulation cases, respectively. It can be seen from Figure 16a that, at each SA, the CO_2 mass fraction tended to increase as the IP increased from 0.01 to 0.02 m in both diesel and DF modes. Meanwhile, at each IP, the CO_2 mass fraction tended to decrease as the SA increased from 40 to 50 degrees in both modes.

Figure 16. CO_2 emissions in all simulation cases: (**a**) CO_2 mass fractions, (**b**) specific CO_2 emissions.

As is widely known, carbon monoxide (CO) and CO_2 are carbon-based emissions, so their formation is directly dependent on the number of carbon (C) atoms contained in the fuel. Moreover, their formation is influenced by the combustion quality inside the engine cylinder. CO_2 is a product of the complete combustion of hydrocarbon fuels. In ICEs, hydrocarbon fuels are firstly oxidized by O_2 contained in the supplied air to form CO during the combustion process. CO then is oxidized to form CO_2 sequentially if there is still enough O_2 and the temperature in the engine cylinder is high enough. In other words, CO_2 formation is strongly influenced by the temperature and O_2 concentration in the engine cylinder.

In this study, as can be seen in Figure 13, at each SA, the in-cylinder peak temperature tended to increase as the IP increased in both diesel and DF modes. The higher temperature inside the engine cylinder promoted the oxidation of CO to form CO_2. This resulted in increases in CO_2 formation as the IP increased in both diesel and DF modes, as shown in Figure 16a. At each IP, as can be seen in Figure 12, the in-cylinder temperature in the 50-degree SA case was the lowest. This resulted in the lowest CO_2 emission formed in this case, as shown in Figure 16a. In the other two cases (40- and 45-degree SA cases), although the peak temperature in both cases was almost the same, the temperature inside the engine cylinder during the expansion process in the 40-degree case was higher than that in the 45-degree case. The higher in-cylinder temperature in this working process of the engine promoted the formation of CO_2 from CO oxidation. This led to an increase in CO_2 formation in the 40-degree case compared with the 45-degree case, as can be observed in Figure 16a.

When expressing the CO_2 emission in terms of specific values, the simulation result showed a different trend as shown in Figure 16b. It can be seen from the figure that the IP of 0.01 m with an SA of 45 degrees produced the lowest specific CO_2 emission in both diesel and DF modes. Using this setting of the injection parameter produced only 0.611 and 0.489 kg/kWh CO_2 emissions in the diesel and DF mode, respectively. This setting of the injection parameter is thus considered to be the optimal parameter that should be set for the fuel injector to reduce CO_2 emissions in both diesel and DF modes.

Compared to the diesel mode, the DF mode helped to reduce CO_2 emissions due to the cleaner characteristics and fewer carbon atoms of NG fuel in comparison to the diesel oil. The reduction tendencies of CO_2 emissions when using NG as the primary fuel in DF modes compared to the diesel mode because of the many advantages of NG had been also reported in much previous research [10–12].

3.6. Wall Heat Flux

Wall heat flux [W/m^2] is the heat energy [J] that fluids (air, exhaust gas, etc.) exchange with walls per unit area [m^2] in a unit of time [s]. Wall heat flux has a positive (+) value if walls transfer heat to fluids; conversely, it has a negative (−) value if walls receive heat from fluids. This means that a negative value of wall heat flux implies heat loss. The wall heat fluxes in all simulation cases are shown in Figure 17. As can be seen in the figure, even though the maximum heat fluxes among the simulation cases were almost the same, there were remarkable differences in wall heat fluxes during the expansion process of the engine. Specifically, at each IP, the wall heat flux tended to decrease as the SA increased from 40 to 50 degrees in both diesel and DF modes. This indicates reductions in heat loss when the SA increases. This is due to the decrease in the temperature inside the engine cylinder during the expansion process as SA increased from 40 to 50 degrees in both cases, as can be seen in Figure 12 and Section 3.3. The reductions in fluid temperature reduced the temperature difference between the fluid and walls. This resulted in a decrease in the wall heat flux and thus a reduction in heat loss through the wall. Compared to the diesel mode, the DF mode has reduced wall heat flux due to the lower in-cylinder temperature during the expansion process of the engine at every IP.
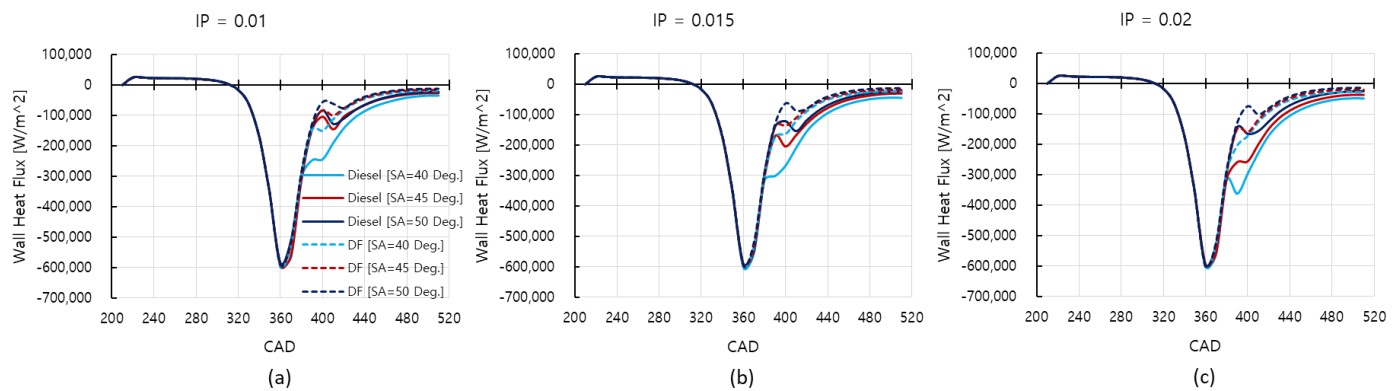
Figure 17. Wall heat fluxes in all simulation cases: (**a**) IP = 0.01 m; (**b**) IP = 0.015 m; (**c**) IP = 0.02 m.

By observing Figure 17, it can also be seen that the IP of 0.01 m has the lowest wall heat flux during the expansion process of the engine in both diesel and DF modes. Therefore, it is highly recommended to use this value for the injector to reduce heat loss due to heat transfer through the engine walls.

4. Conclusions

This study numerically investigated the effects of the SA and IP of the fuel injector on the combustion, performance, and emission characteristics of an ME-GI DF marine engine aiming to find out a set of optimal injection parameters for the injector to reduce engine EGEs.

The major results of the study are as follows:

- The IP of 0.02 m with an SA of 40 degrees produced the highest IMEP for the engine in both diesel and DF modes. This set of injection parameters increased the IMEP of the engine by 11.15% and 6.08% compared to when using the original set of injection parameters (IP = 0.01/SA = 45) in the diesel and DF mode, respectively. It is thus considered to be the optimal parameter that should be set for the fuel injector to enhance engine performance in both diesel and DF modes.
- The IP of 0.01 m with an SA of 50 degrees produced the lowest specific NO emission in both diesel and DF modes. This set of injection parameters decreased the specific NO emissions of the engine by 18.92% and 18.97% compared to when using the original set of injection parameters (IP = 0.01/SA = 45) in the diesel and DF mode, respectively. It is thus considered to be the optimal parameter that should be set for the fuel injector to reduce NO emissions in both diesel and DF modes.

-   The IP of 0.01 m with an SA of 40 degrees produced the lowest specific soot emission in both diesel and DF modes. This set of injection parameters decreased the specific soot emissions of the engine by 23.35% and 16.81% compared to when using the original set of injection parameters (IP = 0.01/SA = 45) in the diesel and DF mode, respectively. It is thus considered to be the optimal parameter that should be set for the fuel injector to reduce soot emissions in both diesel and DF modes.
-   The IP of 0.01 m with an SA of 45 degrees produced the lowest specific CO_2 emission in both diesel and DF modes. This set of injection parameters is thus considered to be the optimal parameters that should be set for the fuel injector to reduce CO_2 emissions in both diesel and DF modes.
-   The IP of 0.01 m helps to reduce heat losses through heat transfer from the combustion gas inside the engine cylinder to the engine combustion chamber walls.

Based on the simulation results presented above, it can be concluded that, even though the IP of 0.02 m with an SA of 40 degrees helps to enhance the engine performance, if the main target is reducing engine exhaust gas emissions, an IP of 0.01 m is highly recommended to be used. At this IP, the specific SA of 40, 45, or 50 degrees that should be used will depend on which emissions need to be reduced.

Appendix A

Appendix A.1. Thermal NO *Formation Reaction Mechanism*

The chemical reaction mechanism calculates the NO formation using the classical Extended Zeldovich scheme as follows [33]:

$$N_2 + O \underset{k_{1b}}{\overset{k_{1f}}{\rightleftarrows}} NO + N \tag{A1}$$

$$N + O_2 \underset{k_{2b}}{\overset{k_{2f}}{\rightleftarrows}} NO + O \tag{A2}$$

$$N + OH \underset{k_{3b}}{\overset{k_{3f}}{\rightleftarrows}} NO + H \tag{A3}$$

with the reaction rates ω_{NO}, for each reaction r considering both the formation and destruction of NO, respectively.

The reaction rate ω_i of each participating species i in the reaction r using the stoichiometric coefficients $\upsilon_{i,r}$ can be written as:

$$\omega_i = \sum_{r=1}^{3} \upsilon_{i,r} \omega_{NO} \tag{A4}$$

Appendix A.2. Thermal NO *Formation Reaction Rates*

The rate constants for these reactions have been measured in numerous experimental studies [51–53], and the data obtained from these studies have been critically evaluated by Baulch et al. [54] and Hanson and Salimian [55]. The expressions for the rate coefficients for Reactions (A1)–(A3) used in the NOx model are given below. These were selected based on the evaluation of Hanson and Salimian [55].

$$k_{1f} = 1.8 \times 10^8 e^{-38370/T} \tag{A5}$$

$$k_{1b} = 3.8 \times 10^7 e^{-425/T} \tag{A6}$$

$$k_{2f} = 1.8 \times 10^4 T e^{-4680/T} \tag{A7}$$

$$k_{2b} = 3.81 \times 10^3 T e^{-20820/T} \tag{A8}$$

$$k_{3f} = 7.1 \times 10^7 e^{-450/T} \tag{A9}$$

$$k_{3b} = 1.7 \times 10^8 e^{-24560/T} \tag{A10}$$

In the above expressions, k_{1f}, k_{2f}, and k_{3f} are the rate constants for the forward Reactions (A1)–(A3), respectively, and k_{1b}, k_{2b}, and k_{3b} are the corresponding reverse rates. All these rates have units of $m^3/gmol.s$.

The net rate of formation of NO via reactions (A1)–(A3) is given by:

$$\frac{d[NO]}{dt} = k_{1f}[O][N_2] + k_{2f}[N][O] + k_{3f}[N][OH] - k_{1b}[NO][N] - k_{2b}[NO][O] \\ - k_{3b}[NO][H] \tag{A11}$$

where all concentrations have units of $gmol/m^3$.

References

1. Thomson, H.; Corbett, J.J.; Winebrake, J.J. Natural gas as a marine fuel. *Energy Policy* **2015**, *87*, 153–167. [CrossRef]
2. Wang, Z.; Zhou, S.; Feng, Y.; Zhu, Y. EGR modeling and fuzzy evaluation of Low-Speed Two-Stroke marine diesel engines. *Sci. Total Environ.* **2020**, *706*, 135444. [CrossRef] [PubMed]
3. Bilgili, L. Life cycle comparison of marine fuels for IMO 2020 Sulphur Cap. *Sci. Total Environ.* **2021**, *774*, 145719. [CrossRef]
4. Nations, U. COVID-19 and maritime transport: Impact and responses. In *United Nations Conference on Trade and Development (UNCTAD)*; Routledge: New York, NY, USA, 2020.
5. Kim, H.J.; Park, S.H.; Lee, C.S. Impact of fuel spray angles and injection timing on the combustion and emission characteristics of a high-speed diesel engine. *Energy* **2016**, *107*, 572–579. [CrossRef]
6. Wei, S.; Ji, K.; Leng, X.; Wang, F.; Liu, X. Numerical simulation on effects of spray angle in a swirl chamber combustion system of DI (direct injection) diesel engines. *Energy* **2014**, *75*, 289–294. [CrossRef]
7. Shu, J.; Fu, J.; Liu, J.; Ma, Y.; Wang, S.; Deng, B.; Zeng, D. Effects of injector spray angle on combustion and emissions characteristics of a natural gas (NG)-diesel dual fuel engine based on CFD coupled with reduced chemical kinetic model. *Appl. Energy* **2019**, *233*, 182–195. [CrossRef]
8. Banapurmath, N.; Marikatti, M.K.; Hunashyal, A.; Tewari, P. Combustion characteristics of a four-stroke CI engine operated on Honge and Jatropha oil methyl ester–ethanol blends when directly injected and dual fuelled with CNG induction. *Int. J. Sustain. Eng.* **2011**, *4*, 145–152. [CrossRef]
9. Decan, G.; Lucchini, T.; D'Errico, G.; Verhelst, S. A novel technique for detailed and time-efficient combustion modeling of fumigated dual-fuel internal combustion engines. *Appl. Therm. Eng.* **2020**, *174*, 115224. [CrossRef]
10. Wei, L.; Geng, P. A review on natural gas/diesel dual fuel combustion, emissions and performance. *Fuel Process. Technol.* **2016**, *142*, 264–278. [CrossRef]
11. Pham, V.C.; Choi, J.-H.; Rho, B.-S.; Kim, J.-S.; Park, K.; Park, S.-K.; Le, V.V.; Lee, W.-J. A numerical study on the combustion process and emission characteristics of a natural gas-diesel dual-fuel marine engine at full load. *Energies* **2021**, *14*, 1342. [CrossRef]
12. Pham, V.C.; Rho, B.-S.; Kim, J.-S.; Lee, W.-J.; Choi, J.-H. Effects of various fuels on combustion and emission characteristics of a four-stroke dual-fuel marine engine. *J. Mar. Sci. Eng.* **2021**, *9*, 1072. [CrossRef]
13. Solutions, M.E. MAN B&W ME-GI Installation in Very Large or Ultra Large Container Vessels. 2450 Copenhagen SV, Denmark, October 2018. Available online: https://www.man-es.com/docs/default-source/document-sync/b-w-me-gi-installation-in-very-large-or-ultra-large-container-vessel-eng.pdf?sfvrsn=2366ce2e_0 (accessed on 8 March 2022).

14. Nemati, A.; Fathi, V.; Barzegar, R.; Khalilarya, S. Numerical investigation of the effect of injection timing under various equivalence ratios on energy and exergy terms in a direct injection SI hydrogen fueled engine. *Int. J. Hydrog. Energy* **2013**, *38*, 1189–1199. [CrossRef]

15. Nehmer, D.A.; Reitz, R.D. Measurement of the effect of injection rate and split injections on diesel engine soot and NOx emissions. *SAE Trans.* **1994**, *103*, 1030–1041.

16. Tow, T.; Pierpont, D.; Reitz, R.D. Reducing particulate and NO x emissions by using multiple injections in a heavy duty DI diesel engine. *SAE Trans.* **1994**, *103*, 1403–1417.

17. Han, Z.; Uludogan, A.; Hampson, G.J.; Reitz, R.D. Mechanism of soot and NOx emission reduction using multiple-injection in a diesel engine. *SAE Trans.* **1996**, *105*, 837–852.

18. Montgomery, D.; Reitz, R.D. Six-mode cycle evaluation of the effect of EGR and multiple injections on particulate and NOx emissions from a DI diesel engine. *SAE Trans.* **1996**, *105*, 356–373.

19. Pierpont, D.; Montgomery, D.; Reitz, R.D. Reducing particulate and NOx using multiple injections and EGR in a DI diesel. *SAE Trans.* **1995**, *104*, 171–183.

20. Nygård, A.; Altimira, M.; Semlitsch, B.; Wittberg, L.P.; Fuchs, L. Analysis of Vortical Structures in Intermittent Jets. In Proceedings of the 5th International Conference on Jets, Wakes and Separated Flows (ICJWSF2015), Stockholm, Denmark, 15–18 June 2015; Springer: Berlin/Heidelberg, Germany, 2016; pp. 3–10.

21. Seol, J.-H.; Pham, V.C.; Lee, W.-J. Effects of the Multiple Injection Strategy on Combustion and Emission Characteristics of a Two-Stroke Marine Engine. *Energies* **2021**, *14*, 6821. [CrossRef]

22. Maghbouli, A.; Yang, W.; An, H.; Li, J.; Shafee, S. Effects of injection strategies and fuel injector configuration on combustion and emission characteristics of a DI diesel engine fueled by bio-diesel. *Renew. Energy* **2015**, *76*, 687–698. [CrossRef]

23. Mobasheri, R.; Peng, Z. *A Computational Investigation into the Effects of Included Spray Angle on Heavy-Duty Diesel Engine Operating Parameters*; SAE Technical Paper; SAE International: Warrendale, PA, USA, 2012; ISSN 0148-7191.

24. Yoon, S.H.; Cha, J.P.; Lee, C.S. An investigation of the effects of spray angle and injection strategy on dimethyl ether (DME) combustion and exhaust emission characteristics in a common-rail diesel engine. *Fuel Process. Technol.* **2010**, *91*, 1364–1372. [CrossRef]

25. Park, S.W.; Reitz, R.D. Optimization of fuel/air mixture formation for stoichiometric diesel combustion using a 2-spray-angle group-hole nozzle. *Fuel* **2009**, *88*, 843–852. [CrossRef]

26. Dolak, J.; Reitz, R. Optimization of the piston geometry of a diesel engine using a two-spray-angle nozzle. *Proc. Inst. Mech. Eng. Part D J. Automob. Eng.* **2011**, *225*, 406–421. [CrossRef]

27. Taghavifar, H.; Taghavifar, H.; Mardani, A.; Mohebbi, A. Exhaust emissions prognostication for DI diesel group-hole injectors using a supervised artificial neural network approach. *Fuel* **2014**, *125*, 81–89. [CrossRef]

28. Siewert, R.M. *Spray Angle and Rail Pressure Study for Low NOx Diesel Combustion*; SAE Technical Paper; SAE International: Warrendale, PA, USA, 2007; ISSN 0148-7191.

29. Kitasei, T.; Yamada, J.; Shoji, T.; Shiino, S.; Mori, K. *Influence of the Different Fuel Spray Wall Impingement Angles on Smoke Emission in a DI-Diesel Engine*; SAE Technical Paper; SAE International: Warrendale, PA, USA, 2008; ISSN 0148-7191.

30. Kim, H.; Reitz, R.D.; Kong, S.-C. *Modeling Combustion and Emissions of HSDI Diesel Engines Using Injectors with Different Included Spray Angles*; SAE Technical Paper; SAE International: Warrendale, PA, USA, 2006; ISSN 0148-7191.

31. Fang, T.; Coverdill, R.E.; Chia-fon, F.L.; White, R.A. Effects of injection angles on combustion processes using multiple injection strategies in an HSDI diesel engine. *Fuel* **2008**, *87*, 3232–3239. [CrossRef]

32. Lim, J.; Min, K. *The Effects of Spray Angle and Piston Bowl Shape on Diesel Engine Soot Emissions Using 3-D CFD Simulation*; SAE Technical Paper; SAE International: Warrendale, PA, USA, 2005; ISSN 0148-7191.

33. ANSYS, Inc. ANSYS Fluent Theory Guide. 2022. Available online: https://www.ansys.com/ (accessed on 8 March 2022).

34. ANSYS, Inc. Geometry Decomposition for Sector Combustion Simulation. Volume Fluent 19.2. 2022. Available online: https://www.ansys.com/ (accessed on 8 March 2022).

35. National Center for Biotechnology Information. PubChem Compound. Decane–Compound Summary. Available online: https://pubchem.ncbi.nlm.nih.gov/compound/Decane (accessed on 25 February 2022).

36. Friend, D.G.; Ely, J.F.; Ingham, H. Thermophysical properties of methane. *J. Phys. Chem. Ref. Data* **1989**, *18*, 583–638. [CrossRef]

37. Durbin, P.A. Near-wall turbulence closure modeling without "damping functions". *Theor. Comput. Fluid Dyn.* **1991**, *3*, 1–13.

38. Jia, L.; Yu, Y.; Li, Z.-P.; Qin, S.-N.; Guo, J.-R.; Zhang, Y.-Q.; Wang, J.-C.; Zhang, J.-C.; Fan, B.-G.; Jin, Y. Study on the Hg0 removal characteristics and synergistic mechanism of iron-based modified biochar doped with multiple metals. *Bioresour. Technol.* **2021**, *332*, 125086. [CrossRef]

39. Pope, S.B. PDF methods for turbulent reactive flows. *Prog. Energy Combust. Sci.* **1985**, *11*, 119–192. [CrossRef]

40. Rao, V.; Honnery, D. A comparison of two NOx prediction schemes for use in diesel engine thermodynamic modelling. *Fuel* **2013**, *107*, 662–670. [CrossRef]

41. Brookes, S.; Moss, J. Predictions of soot and thermal radiation properties in confined turbulent jet diffusion flames. *Combust. Flame* **1999**, *116*, 486–503. [CrossRef]

42. Kong, S.-C.; Reitz, R. Use of detailed chemical kinetics to study HCCI engine combustion with consideration of turbulent mixing effects. *J. Eng. Gas. Turbines Power* **2002**, *124*, 702–707. [CrossRef]

43. Montazeri, H.; Blocken, B. CFD simulation of wind-induced pressure coefficients on buildings with and without balconies: Validation and sensitivity analysis. *Build. Environ.* **2013**, *60*, 137–149. [CrossRef]
44. Meng, F.-Q.; He, B.-J.; Zhu, J.; Zhao, D.-X.; Darko, A.; Zhao, Z.-Q. Sensitivity analysis of wind pressure coefficients on CAARC standard tall buildings in CFD simulations. *J. Build. Eng.* **2018**, *16*, 146–158. [CrossRef]
45. Celik, I.B.G.U.; Roache, P.J.; Freitas, C.J.; Coleman, H.; Raad, P.E. Procedure for Estimation and Reporting of Uncertainty Due to Discretization in CFD Applications. *J. Fluids Eng.* **2008**, *130*, 078001-1–078001-4.
46. Savli, M. *Turbulence Kinetic Energy–TKE*; Faculty of Mathematics and Physics, University of Ljubljana: Ljubljana, Slovenia, 2012; p. 9.
47. Heywood, J.B. *Internal Combustion Engine Fundamentals*; McGraw-Hill Education: New York, NY, USA, 1998.
48. Shahbaz, M.; Jüngst, N.; Grzeszik, R.; Kaiser, S. Endoscopic fuel film, chemiluminescence, and soot incandescence imaging in a direct-injection spark-ignition engine. *Proc. Combust. Inst.* **2021**, *38*, 5869–5877. [CrossRef]
49. Mansurov, Z. Combust. Explos. *Shock Waves* **2005**, *41*, 727–744. [CrossRef]
50. Zhang, Q.; Li, M.; Shao, S. Combustion process and emissions of a heavy-duty engine fueled with directly injected natural gas and pilot diesel. *Appl. Energy* **2015**, *157*, 217–228. [CrossRef]
51. Blauwens, J.; Smets, B.; Peeters, J. Mechanism of "prompt" no formation in hydrocarbon flames. *Symp. (Int.) Combust.* **1977**, *16*, 1055–1064. [CrossRef]
52. Flower, W.L.; Hanson, R.K.; Kruger, C.H. Kinetics of the reaction of nitric oxide with hydrogen. *Symp. (Int.) Combust.* **1975**, *15*, 823–832. [CrossRef]
53. Monat, J.P.; Hanson, R.K.; Kruger, C.H. Shock tube determination of the rate coefficient for the reaction $N_2 + O \rightarrow NO + N$. *Symp. (Int.) Combust.* **1979**, *17*, 543–552. [CrossRef]
54. Baulch, D.; Drysdale, D.; Horne, D.; Lloyd, A. *Evaluated Kinetic Data for High Temperature Reactions*; Butterworths: London, UK, 1973; Volumes 1–2.
55. Hanson, R.K.; Salimian, S. Survey of rate constants in the N/H/O system. In *Combustion Chemistry*; Springer: Berlin/Heidelberg, Germany, 1984; pp. 361–421.